Intramolecular Charge Transfer in 5-Methoxy-2-(2-pyridyl)thiazole-Derived Fluorescent Molecules with Different Acceptor or Donor Substituents

Wei Sun, Can Zhou, Chun-Hu Xu, Yi-Qun Zhang, Zhan-Xian Li, Chen-Jie Fang, Ling-Dong Sun, and Chun-Hua Yan*

Beijing National Laboratory for Molecular Sciences, State Key Laboratory of Rare Earth Materials Chemistry and Applications and PKU-HKU Joint Laboratory in Rare Earth Materials and Bioinorganic Chemistry, Peking University, Beijing 100871, China

Received: January 23, 2009; Revised Manuscript Received: June 18, 2009

On the basis of the rational derivation of 5-methoxy-2-(2-pyridyl)thiazole (2-MPT), we synthesized a new series of charge-transfer-based fluorescent molecules bearing different electronic donors or acceptors. The substituents range from strong electronic donors (e.g., amino and hydroxyl groups) to weak donating groups (e.g., proton and methyl groups) and electronic acceptors (e.g., pyridine ring). Through systematic investigation on the substituent-/polarity-dependent spectra (including room-temperature absorption, room-/low-temperature steady-state fluorescence spectra, and transient fluorescence lifetime characterization) and theoretical calculations, the emission properties of MPT derivatives are found to be governed by the rotation of the substituent around the triple bond axis, which produces distinct intramolecular charge transfer processes in either the twisted or planar excited states. The interconversion of excited-state geometry triggered by local interactions in polar solvents may produce a bathochromic shift of approximately 100 nm in fluorescence spectra. The solution state may also affect the ground- and excited-state conformation and hence results in the solvent-frozen-point sensitive fluorescence for some of the as-prepared molecules.

Introduction

Recent development in molecular optical biolabels, sensors, and logic gates offers a great challenge for the design and synthesis of novel molecular switches, which contain particular recognition sites for exhibiting optical or electrical response to the external stimuli, such as ion, electricity, or irradiation.[1−3] In particular, when the molecular switch utilizes fluorescence as an optical output channel, the changes in either fluorescence intensity or emission position provide zero-background output signal[4] and single-molecule resolution[5] in sensing applications. One common way to synthesize new molecular fluorescence switches in current is to derive the fluorophore with preorganized reception sites, which can bind to specific proteins, guest molecules, or ions.[2d,4b] However, the modulation of the fluorophore by reception sites also brings distinct interplay effects between the fluorophore and the reception site at both the ground and excited states. As an example, the electron-rich metal binding sites, such as hydroxyl group or amino group, may donate electrons to the originally fluorophore-centered frontier orbitals at the excited states, whereas the electron-deficient binding groups, such as the pyridine ring, may accept electrons from the fluorophore.[2d,6] Consequently, the charge transfer processes triggered by the cooperation between the fluorophore and the reception site produce new fluorescence switching features. Furthermore, the substituent may also affect the structural stabilization energy of fluorescent molecules via interactions with solvent molecules, thus adding the uncertainty to the fluorescence property after derivation.[7] Therefore, investigating the derivation−fluorescence correlation by reception site is a key issue for employing a fluorophore in potential optical sensing applications.

5-Methoxy-2-(2-pyridyl)thiazole (2-MPT) is a newly developed blue-emissive fluorophore with high quantum yield in both water and common organic solvents.[8] The existence of coordination sites, such as pyridine ring and thiazole ring in 2-MPT, also makes it a potential fluorescent molecule for proton and metal ions. On the basis of the cooperation between coordination and irradiation/redox processes, several binary logic gates have been implemented within 2-MPT derivatives.[9] However, further investigations on the application potential of MPT-derived fluorescence switches in molecular sensors and logic circuits require detailed understanding on the perturbation of original MPT-centered charge transfer by the reception site.

In this work, we report the photophysical properties in the donor- or acceptor-derived 2-MPT fluorescent molecules (Scheme 1). The related compounds are with similar molecular framework, in which the fluorophore and the aromatic substituent are covalently linked to a triple bond. The electronic nature of substitution groups is systematically varied from the strong electron donors (e.g., hydroxyl group and amino groups) to weak donors (e.g., methyl group and hydrogen atom) and even electron acceptors (e.g., pyridine ring). Both the spectral and theoretical investigations have revealed different roles of the substituents in the electronic transitions in 2-MPT derivatives. The conformation relaxation of a twisted Franck−Condon excited state to either a twisted or a coplanar structure endows the related fluorescent molecules through the relative rotation of the introduced aromatic ring around the triple bond axis with distinct fluorescence properties, from an emission band at around 435 nm in relaxed twisted intramolecular charge transfer (TICT) excited state to an emission band at 560 nm in relaxed planar intramolecular charge transfer (PICT) excited state. The existence of the electronic donating substituent allows the active site to increase substituent−solvent interactions. The activation of

* Corresponding author. E-mail: yan@pku.edu.cn.

10.1021/jp9007224 CCC: $40.75
Published on Web 07/08/2009

SCHEME 1: Chemical Structures of Related MPT Derivatives

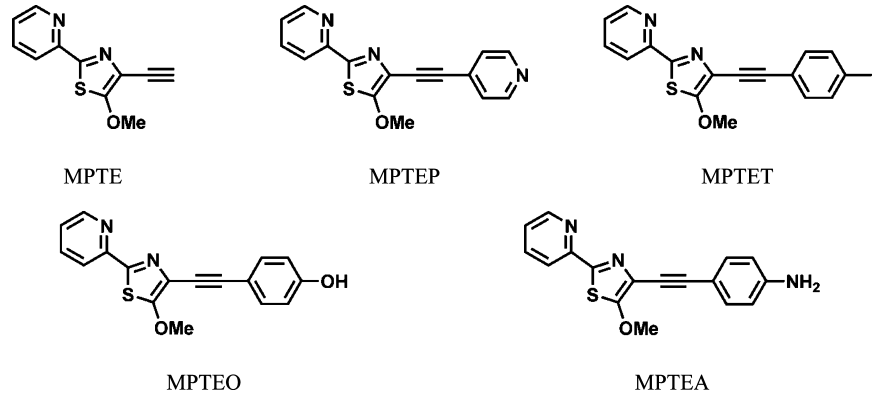

the rotation freedom is also sensitive to the solvent polarity and the solution state. When temperature is kept below the frozen point, the PICT emission at 560 nm is activated for some of the as-prepared molecules with a solution-phase-sensitive fluorescence switching.

Experimental Section

Materials. All reagents were purchased from commercial sources and used without further purification. All reactions were performed under an argon atmosphere using purified solvents by standard methods. For chromatography, 160−200 mesh silica gel (Qingdao, China) was used.

Apparatus. Mass spectra were recorded on a ZAB-HS mass spectrometer. NMR spectra were recorded on a Varian Mercury 400 spectrometer. Chemical shifts were reported in ppm using tetramethylsilane (TMS) as the internal standard. IR spectra were recorded on a Nicolet 5MX-S infrared spectrometer.

Spectroscopic Characterization. The solvents for the spectroscopic measurements, such as *n*-hexane (Hex), toluene (Tol), ethylacetate (EA), dichloromethane (DCM), acetonitrile (AN), acetone (Ace), and *N*,*N*-dimethylformamide (DMF), were all HPLC grade and used without further purification. No spectral impurity was found in the interested wavelength region in either absorption or fluorescence. The concentrations of the substrate and chemical inputs are listed in the footnotes of corresponding Figures.

UV−vis absorption spectra were measured with a Shimadzu UV-3100 spectrometer, and the steady-state fluorescence spectra were recorded upon the excitation at 350 nm (Xe lamp in the F-4500 spectrometer) on a Hitachi F-4500 fluorescence spectrometer.

The fluorescence quantum yields were determined following eq 1[10] with quinine bisulfate in 1 M H_2SO_4 ($\Phi_{fr} = 0.546$) solution as the reference. Φ_{fr} and Φ_r are the quantum yield of the reference and the test sample, respectively; A_r and A are the absorbance at the excitation wavelength of the reference and the test sample, respectively; L_r and L are the light path length in the absorption cells of the reference and the test sample, respectively; N_r and N are the indexes of refraction of the solvents in the reference sample and the test sample, respectively; and D_r and D are the integrated areas of the emission peaks of the reference and the test sample, respectively. Sample and reference were prepared with absorbance of 0.1 at the excitation wavelength.

$$\Phi = \Phi_{fr} \times \frac{1 - 10^{-A_r L_r}}{1 - 10^{-AL}} \times \frac{N^2}{N_r^2} \times \frac{D}{D_r} \qquad (1)$$

The low-temperature fluorescence signals were recorded on a Jobin-Yvon HR800 Raman spectrometer (France) with a 325 nm laser excitation source.

The fluorescence lifetimes were obtained from an Edinburgh LifeSpec-Red ps fluorescence lifetime spectrometer.

Syntheses. MPTE and MPTEA were prepared following the previous report by us.[9b,d]

MPTET. The synthesis of MPTET follows the same reaction procedures as those of MPTEA, except the reagent 4-iodo-aniline is replaced by 4-iodo-toluene. Yield: 65%. HRMS (*m*/*z*): calcd for $C_{18}H_{14}N_2OS$, 306.0827; found, 306.0830. ^{1}H NMR (in $CDCl_3$, 400 MHz, δ): 8.55 (d, 1H), 8.14 (d, 1H), 7.78 (m, 1H), 7.48 (d, 2H), 7.29 (m, 1H), 7.15 (d, 2H), 4.15 (s, 3H), 2.37 (s, 3H) (Figure S1a in the Supporting Information). ^{13}C NMR (in $CDCl_3$, 100 MHz, δ): 166.2, 153.0, 150.1, 148.1, 137.6, 136.0, 130.6, 128.0, 123.1, 119.3, 118.8, 117.9, 92.4, 79.5, 62.6, 20.5. FT-IR (in KBr) υ (cm^{-1}): 3021 (m), 2211 (m), 1586 (s), 1564 (m), 1529 (s), 1497 (vs), 1453 (m), 1435 (s), 1357 (vs), 1244 (s), 1215 (m), 1166 (m), 1019 (s), 998 (s), 953 (m), 812 (s), 779 (s).

MPTEO. The synthesis of MPTEO follows the same reaction procedures as those of MPTEA, except the reagent 4-iodo-aniline is substituted by 4-iodo-phenol. Yield: 44%. HRMS (*m*/*z*): calcd for $C_{17}H_{12}N_2O_2S$, 308.0620; found, 308.0620. ^{1}H NMR (in actone-d6, 400 MHz, δ): 8.53 (d, 1H), 8.14 (d, 1H), 7.76 (t, 1H), 7.46 (d, 2H), 7.27 (t, 1H), 6.81 (d, 2H), 5.41 (s, 1H), 4.14 (s, 3H) (Figure S1b in the Supporting Information). ^{13}C NMR (in acetone-d_6, 100 MHz, δ): 167.2, 157.9, 153.6, 151.0, 149.3, 137.2, 132.9, 124.3, 120.1, 118.2, 115.6, 113.7, 92.6, 79.8, 63.3. FT-IR (in KBr) υ (cm^{-1}): 3500−2400 (m), 2213 (m), 1606 (s), 1586 (s), 1538 (vs), 1508 (vs), 1494 (vs), 1435 (s), 1355 (vs), 1268 (vs), 1245 (s), 1166 (m), 1027 (m), 957 (s), 831 (s), 786 (s).

MPTEP. The synthesis of MPTEP follows the same reaction procedures as those of MPTEA, except the reagent 4-iodo-aniline is replaced by 4-bromo-pyridine hydrochloride. Yield: 30%. HRMS (*m*/*z*): calcd for $C_{16}H_{11}N_3OS$, 293.0623; found, 293.0628. ^{1}H NMR (in $CDCl_3$, 400 MHz, δ): 8.61 (d, 2H), 8.55 (d, 1H), 8.14 (d, 1H), 7.79 (m, 1H), 7.47 (d, 2H), 7.31 (m, 1H), 4.17 (s, 3H) (Figure S1c in the Supporting Information). ^{13}C NMR (in $CDCl_3$, 100 MHz, δ): 169.2, 154.5, 150.8, 149.4, 149.2, 137.0, 128.8, 125.4, 124.3, 118.8, 118.7, 90.5, 86.3, 63.7. FT-IR (in KBr) υ (cm^{-1}): 3028 (w), 2925 (w), 2212 (s), 1594 (s), 1519 (vs), 1490 (s), 1434 (s), 1364 (vs), 1251 (s), 1218 (m), 1211 (m), 1026 (m), 993 (s), 954 (m), 814 (s), 775 (s).

Quantum Chemistry Calculation. Geometry optimization for the MPT derivatives were carried out with Gaussian 03 software[11] (Gaussian Inc.) at the B3LYP/6-31G(d,p) level by

DFT theory. The adiabatic electronic transitions for the related 2-MPT derivatives in solvents were performed at the MPW1PW91/6-31G+(d,p) level with TD-DFT theory using Gaussian 03 software. Charge distribution for the related fluorescent molecules was calculated at the RCIS/6-311G(d,p) level using Gaussian 03 software.[12] The solvent effect has been considered using the polarizable continuum model (PCM).

Results and Discussion

Absorption. Figure 1 shows the steady-state absorption and fluorescence spectra of MPTE, MPTEP, MPTET, MPTEO, and MPTEA in selective solvents. Selected spectral data are also listed in Table 1.

As shown in Figure 1, the high extinction coefficient of the related absorption peaks indicates that the related electronic transitions are originated from $\pi \rightarrow \pi^*$ orbital excitation, and the less structured absorption peaks in all related solvents indicate the electronic transitions with charge transfer (CT) nature.[13] The similarity of both the band shape and absorption wavelength for MPTE at 334 nm and 2-MPT at 320 nm in acetonitrile reveals the similar ground-state geometries for both 2-MPT and MPTE and suggests that the first intense absorption generates from the $S_0 \rightarrow S_1$ electronic transition of MPTE.[8] This suggests that the introduction of a rigid triple bond to MPT skeleton does not significantly affect the ground-state conformation. The slight bathochromic shift of maximum absorption wavelength of MPTE compared with that of 2-MPT also indicates the lowering of the frontier orbital energy gap by the extension of frontier orbitals via the π-nature orbitals of the triple bond.

As for MPTEP, one intense $S_0 \rightarrow S_2$ transition is found at 320 nm with a shoulder peak corresponding to the $S_0 \rightarrow S_1$ transition at 348 nm in the apolar solvent *n*-hexane. Whereas in polar solvents, such as acetonitrile and dichloromethane, only a pseudo one-peak band is observed at around 326 nm. However, the deconvolved absorption spectrum in acetonitrile further reveals that two slightly separated peaks that correspond to $S_0 \rightarrow S_1$ and $S_0 \rightarrow S_2$ emerge at 345 and 319 nm, respectively (Figure S2 in the Supporting Information). The extinction coefficient ratio of the two deconvolved peaks is 0.42.

As for MPTET, MPTEO, and MPTEA, they exhibit similar absorption peaks. The absorption peaks corresponding to the $S_0 \rightarrow S_1$ electronic transition in acetonitrile appear at 343, 344, and 356 nm, respectively. Another absorption peak corresponding to the $S_0 \rightarrow S_3$ electronic transition appears at 295, 294, and 309 nm, respectively, with a shoulder peak corresponding to $S_0 \rightarrow S_2$ emerging at 308, 310, and 326 nm, respectively. The similarity in absorption spectra among MPTET, MPTEO, and MPTEA suggests similar ground-state conformation, although some derivations may be ascribed to the differences in detailed structural parameters or electronic donating strength. Compared with that of 2-MPT and MPTE, the changes in absorption spectra also illustrate that the aromatic ring in MPTEP, MPTET, MPTEO, and MPTEA is strongly coupled to the MPT moiety at the ground state. Both the acylation (Figure S3 in the Supporting Information) and protonation[9d] at the amino group reduce the electron donating ability of the lone electron pair and blue shift the absorption corresponding to the $S_0 \rightarrow S_1$ transition in MPTEA to some extent with significant changes of band shape, which implies the contribution of the lone electron pair of the electron-donating substituent to HOMO of MPTEA at the ground state.[14] The assignments for the absorption peaks as excitation from the ground state S_0 to the excited state S_n in the related fluorescent molecules are further confirmed by theoretical calculation results listed below.

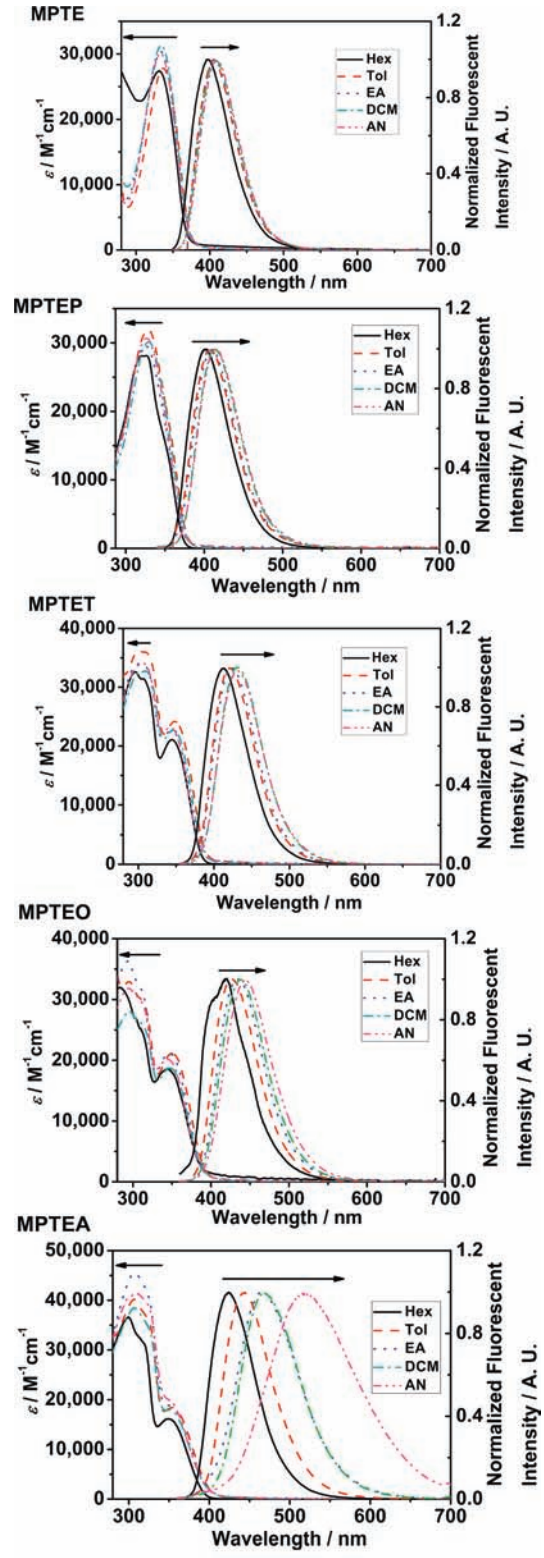

Figure 1. Absorption and fluorescence spectra of the related MPT derivatives in different solvents. The left scale bar in each figure represents the extinction coefficient, and the right scale bar represents the normalized fluorescence intensity.

When solvent polarity increases, the absorption wavelength for the $S_0 \rightarrow S_1$ transition is slightly shifted for the related fluorescent molecules, indicating a small difference between the ground-state molecular dipole moment and the Franck−Condon

TABLE 1: Selective Absorption and Fluorescence Data of the Related MPT Derivatives in Different Solvents

fluorescent molecule	parameter	*n*-hexane	toluene	ethylacetate	dichloromethane	acetonitrile
MPTE	λ_{abs}/nm	330	337	334	335	334
	$\log(\varepsilon_{max}/M^{-1}\cdot cm^{-1})$	4.4	4.4	4.5	4.5	4.5
	λ_{em}/nm	397	405	406	408	410
	Φ_{FL}	0.024	0.080	0.083	0.076	0.082
	ΔS/nm	67	68	72	73	76
	τ/ns	0.48	0.24	0.43	0.42	0.43
MPTEP	λ_{abs}/nm	320	328	325	326	326
	$\log(\varepsilon_{max}/M^{-1}\cdot cm^{-1})$	4.4	4.5	4.5	4.5	4.5
	λ_{em}/nm	401	407	408	413	415
	Φ_{FL}	0.035	0.047	0.042	0.033	0.021
	ΔS/nm	81	79	83	87	89
	τ/ns	0.28	0.28	0.21	0.22	0.20
MPTET	λ_{abs}/nm	344, 308, 295	348, 310, 300	345, 306, 298	345, 310, 299	343, 308, 295
	$\log(\varepsilon_{max}/M^{-1}\cdot cm^{-1})$	4.3, 4.5, 4.5	4.4, 4.5, 4.5	4.4, 4.5, 4.5	4.4, 4.5, 4.5	4.4, 4.5, 4.5
	λ_{em}/nm	412	420	423	431	432
	Φ_{FL}	0.031	0.037	0.032	0.031	0.031
	ΔS/nm	68	72	78	86	89
	τ/ns	0.23	0.25	0.26	0.25	0.25
MPTEO	λ_{abs}/nm	344, 312, 283	350, 311, 295	347, 309, 293	347, 310, 295	344, 310, 294
	$\log(\varepsilon_{max}/M^{-1}\cdot cm^{-1})$	4.3, 4.4, 4.5	4.3, 4.5, 4.5	4.3, 4.5, 4.6	4.3, 4.4, 4.4	4.3, 4.5, 4.5
	λ_{em}/nm	418	426	434	439	444
	Φ_{FL}	0.020	0.026	0.025	0.025	0.023
	ΔS/nm	74	76	87	92	100
	τ/ns	0.40[a]	0.25	0.25	0.25	0.26
MPTEA	λ_{abs}/nm	349, 318, 298	354, 325, 307	352, 325, 307	351, 324, 307	356, 326, 309
	$\log(\varepsilon_{max}/M^{-1}\cdot cm^{-1})$	4.2, 4.5, 4.6	4.3, 4.6, 4.6	4.3, 4.6, 4.7	4.3, 4.5, 4.6	4.3, 4.6, 4.6
	λ_{em}/nm	424	444	465	470	520
	Φ_{FL}	0.026	0.026	0.024	0.026	0.020
	ΔS/nm	75	90	113	119	164
	τ/ns	0.25	0.27	0.25	0.39	1.21

[a] Lifetime of MPTEO in *n*-hexane is fitted double-exponentially and reported as the average lifetime.[7a]

excited state for each fluorescent molecule, whatever the substituent is.

Room-Temperature Fluorescence. Each MPT-derived fluorescent molecule exhibits a single-peak emission band when excited at the UV region. The excitation spectrum of each fluorescent molecule matches its absorption spectrum in the employed solvent, which indicates that the emission originates from a single molecular emission process (Figure S4 in the Supporting Information). The excitation of the $S_0 \rightarrow S_1$ transition directly triggers the emission band, suggesting that the fluorescence originates from the $S_1 \rightarrow S_0$ deactivation process. In each specific solvent, the emission wavelength increases in a sequence of MPTE < MPTEP < MPTET < MPTEO < MPTEA. As for the molecules with an electronic donating substituent, the emission wavelength is red-shifted from 432 nm in MPTET to 520 nm in MPTEA in acetonitrile, which suggests that the stronger electronic donor tends to produce a larger excited-state molecular dipole moment, and even in the nonpolar *n*-hexane, the emission wavelength is increased in a sequence as MPTET < MPTEO < MPTEA. When the amino group of MPTEA is acylated in acetonitrile, the emission band is largely hypsochromic shifted from 520 to 435 nm, which further confirms the effect of electronic donators.[9d]

The correlation between the emission wavelength and the solvent polarity is also dependent on the nature of the substituent. For MPTE, MPTEP, MPTET, and MPTEO, the emission peak is slightly red-shifted with the increase in solvent polarity, whereas for MPTEA, the emission wavelength is strongly dependent on the solvent polarity and ranges from 424 nm in *n*-hexane to 532 nm in DMF. The red-shifted fluorescence of MPTEA retains the same excitation spectra as those in 424 nm (Figure S4 in the Supporting Information), suggesting that solvent polarity does not introduce new excitation pathways besides the original $S_0 \rightarrow S_1$ excitation process.

The excited-state dipole moment can be calculated from eq 2,[15] in which the emission wavenumber is found to be a function of solvent polarity parameter, f'.

$$\nu_f = -(1/2\pi\varepsilon_0 hca^3)[\mu_e(\mu_e - \mu_g)]f' + \text{const} \qquad (2)$$

where

$$f' = \left(\frac{\varepsilon - 1}{2\varepsilon + 1}\right) - \left(\frac{n^2 - 1}{4n^2 + 2}\right) \qquad (3)$$

ν_f represents the maximum fluorescence wavenumber; μ_g and μ_e represent the ground-state and excited molecular dipole moments, respectively; μ_g is derived from DFT calculations, as discussed in the following sections; a is the Onsager solvent cavity radius, which is calculated from DFT calculations; and ε, ε_0, and n are the dielectric constant of solvent, the vacuum dielectric constant, and the solvent refractive index, respectively.

From this plot (Figure 2), one single fitting line is obtained for MPTE, MPTEP, MPTET, and MPTEO, resulting in the excited-state molecular dipole moment less than 6.5 D, as listed in Table 2. Because of the abnormal fluorescence red shift of MPTEA in polar solvents, the plot for MPTEA is best fitted by two lines with distinct slopes. In the low solvent polarity parameter region, such as *n*-hexane, toluene, and ethylacetate, the excited-state molecular dipole moment of MPTEA is around 9.17 D, whereas in the high solvent polarity parameter region, such as acetonitrile and DMF, the excited-state molecular dipole moment of MPTEA is increased to around 17.27 D. The relaxed excited dipole for all MPTE, MPTEP, MPTET, MPTEO, and MPTEA (low f' region) is slightly larger than the Franck−Condon excited dipole, whereas the relaxed excited dipole for MPTEA

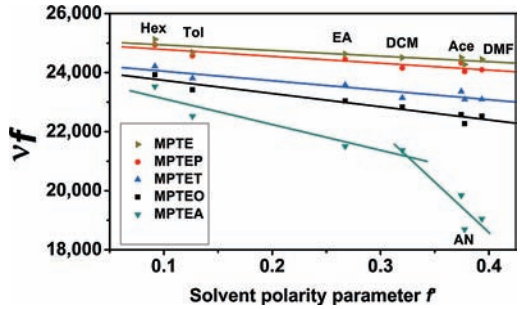

Figure 2. Plot of room-temperature fluorescence wavenumber versus solvent polarity parameter (Mataga plot). Hex: *n*-hexane; Tol: toluene; EA: ethylacetate; DCM: dichloromethane; Ace: acetone; AN: acetonitrile; DMF: *N*,*N*-dimethylformamide.

TABLE 2: Slope for the Fluorescence Wavelength of Related MPT Derivatives Versus the Polarity Parameter and the Excited Molecular Dipole Moment

fluorescent molecule	*a*/Å[a]	μ_g/debye[b]	slope for polarity plot/cm^{-1}	μ_e/debye[c]	μ_e^{FC}/debye[d]
MPTE	4.68	0.8119	1896	3.24	3.28
MPTEP	5.13	2.2896	2327	4.81	4.20
MPTET	5.64	1.7598	3209	5.62	4.10
MPTEO	5.26	2.0489	4469	6.14	4.25
MPTEA (low f' region)	5.23	3.7417	8720	9.17	6.86
MPTEA (high f' region)	5.23	3.7417	34 209	17.27	6.86

[a] Onsager radius, obtained from DFT calculation. [b] Ground-state dipole moment, obtained from DFT calculation. [c] Excited-state dipole moment. [d] Franck−Condon excited-state dipole moment, calculated from Lippert equation.[15b]

(high f' region) is two times larger than the Franck−Condon excited dipole. This is ascribed to the excited-state conformation relaxation of MPTEA, which is produced by the relaxation of the Franck−Condon excited state to increase the dipole moment for more solvent stabilization energy in polar solvents. The relaxed excited-state dipole moment value increases in a sequence as MPTE < MPTEP < MPTET < MPTEO < MPTEA (low f' region) < MPTEA (high f' region). In particular, the drastic change of excited dipole moment between MPTEO and MPTEA at high f' region indicates that their relaxed excited-state geometry is different in polar solvents, considering their similar ground-state structures and electronic donating strength. Therefore, other substitution effects besides the electronic donating strength may contribute to stabilizing the relaxed charge-separated excited-state conformation.

Further spectral characterization for MPTEA has also been executed. In the dichloromethane solution of MPTEA, the introduction of a small amount of acetonitrile (no more than 5%) gradually produces red shift of emission band from 470 to around 500 nm (Figure 3). The existence of the isobastic point indicates that the red shift is due to the formation of a new emission band, which reveals a dual-state model for MPTEA in a different solvent environment, and both of the relaxed excited states are generated from the same Franck−Condon excited state,[14] considering that the fluorescence is triggered through the direct excitation of MPTEA from S_0 to S_1. Notably, the amount of acetonitrile does not produce significant perturbation of solvent polarity or viscosity, indicating that the large dipole excited-state conformation of MPTEA is acetonitrile-specific sensitive, and the formation of the large dipole excited state is controlled by the solvent viscosity. In poly(ethylene glycol) (PEG) solution of MPTEA with both large polarity and viscosity, the formation of a large dipole excited state is prohibited, which produces an emission band centered at 435 nm (Figure S5 in the Supporting Information). However, when PEG solution of MPTEA is added with 5% volume ratio of acetonitrile, the emission at 435 nm is decreased, whereas the emission at around 510 nm is largely increased, similar to those that happened in the dichloromethane/acetonitrile mixture.

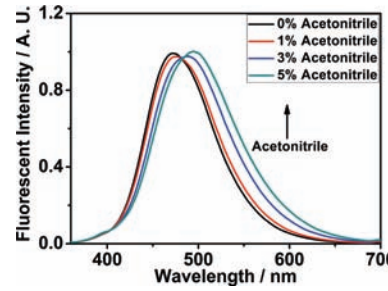

Figure 3. Fluorescence spectra of MPTEA in dichloromethane, to which acetonitrile was added. The volume concentration of acetonitrile to dichloromethane is 0, 1, 3, and 5%. Concentration of MPTEA is 0.02 mM.

Fluorescence Quantum Yield and Fluorescence Lifetime. The derivation at MPT moiety also affects the fluorescence quantum yield and the fluorescence lifetime, as presented in Table 1. Compared with that of 2-MPT, the fluorescence quantum yields of the derivatives are largely reduced, indicating that the introduction of additional substituent promotes new nonradiative energy transfer pathways at the excited state. For MPTE and MPTEP, the fluorescence quantum yield is sensitive to the solvent polarity. The fluorescence quantum yield for MPTE increases alongside the solvent polarity, whereas for MPTEP, it is significantly decreased. For the derivatives bearing an electron donor, such as MPTET, MPTEO, and MPTEA, the fluorescence quantum yield only shows small solvent polarity dependence and maintains an approximate value in the majority of researched solvents.

In most cases, the lifetimes of the related molecules are best fitted monoexponentially, except MPTEO in *n*-hexane. This suggests only one relaxation pathway from Franck−Condon excited state in pure solvent, and the relaxed excited state with large dipole moment is not generated from the one with the smaller excited dipole moment. Otherwise, a double-exponential lifetime should exist in polar solvents, for example, acetonitrile. However, in the mixture solvent of dichloromethane and acetonitrile (v/v 19:1), the lifetimes at different wavelengths are best fitted double-exponentially (Table S1 in the Supporting Information). One fitted lifetime is about 0.18 ns, and another is about 0.75 ns. The contribution of each lifetime item is variable depending on the emission wavelength, which coincides with the dual-state model for the excited MPTEA in mixture solvent. At longer wavelength, the contribution of emission processes with 0.75 ns lifetime is also increased, revealing that the excited state with the larger dipole moment emits at longer wavelength. Therefore, in the mixture solvent, a same Franck−Condon excited state is transformed to two distinct relaxed excited states in different solvent environments, considering that the single solvent environment produces only a unique relaxed excited state. For MPTE, the lifetime is reduced one-half in toluene compared with that in *n*-hexane but recovers in polar solvents, for example, dichloromethane and acetonitrile. For MPTEP, MPTET, and MPTEO, their lifetimes are nearly constant when the solvent polarity increases, whereas the lifetime for MPTEA is increased to be four times that in *n*-hexane.

TABLE 3: Fluorescence Rate Constant (k_f) and the Nonradiative Deactivation Rate Constant (k_{nr}) of the Related MPT Derivatives in Different Solvents

fluorescent molecule	rate constant	*n*-hexane	toluene	ethyl acetate	dichloromethane	acetonitrile
MPTE	$k_f/10^9\ s^{-1}$	0.050	0.33	0.19	0.18	0.19
	$k_{nr}/10^9\ s^{-1}$	2.3	2.4	2.1	2.2	1.8
MPTEP	$k_f/10^9\ s^{-1}$	0.12	0.17	0.2	0.15	0.10
	$k_{nr}/10^9\ s^{-1}$	3.4	3.4	4.6	4.4	4.9
MPTET	$k_f/10^9\ s^{-1}$	0.13	0.15	0.12	0.12	0.12
	$k_{nr}/10^9\ s^{-1}$	4.2	3.8	3.7	3.9	3.9
MPTEO	$k_f/10^9\ s^{-1}$	0.050	0.10	0.10	0.10	0.088
	$k_{nr}/10^9\ s^{-1}$	2.4	3.9	3.9	3.9	3.8
MPTEA	$k_f/10^9\ s^{-1}$	0.10	0.096	0.096	0.067	0.016
	$k_{nr}/10^9\ s^{-1}$	3.9	3.6	3.9	2.5	0.81

As calculated from eqs 4 and 5, the fluorescence rate constant (k_f) of MPTE is increased by three times from apolar *n*-hexane to polar acetonitrile (Table 3), and the nonradiative deactivation rate constant (k_{nr}) value is decreased by about one-fourth. In contrast, the k_f value decreases for MPTEP when the solvent polarity is increased, whereas k_{nr} value increases. This suggests a less stable excited state in polar solvents. For MPTET and MPTEO, k_f and k_{nr} values slightly change from apolar *n*-hexane to polar acetonitrile. For MPTEA, values of both k_f and k_{nr} dramatically decreased when the solvent was changed from *n*-hexane to acetonitrile. The large decrease in k_f for MPTEA indicates that the S_1 excited-state geometry in polar solvent must relax to a distinct conformation from that in the apolar solvent. However, in less polar solvents, for example, toluene and ethyl acetate, the values of both k_f and k_{nr} remain approximately the same as those of MPTET and MPTEO. This suggests a similar S_1 excited-state geometry for MPTET, MPTEO, and MPTEA. The excited-state conformation transformation may only occur at polar solvents with a large dipole moment at room temperature.

$$k_f = \frac{\Phi_f}{\tau_f} \qquad \text{(ref 16)} \tag{4}$$

$$k_{nr} = \frac{1 - \Phi_f}{\tau_f} \tag{5}$$

Frozen Solution Fluorescence. The emission properties of MPT derivatives bearing an aromatic substituent are also sensitive to the phase state of solution, that is, liquid or frozen state. When acetonitrile solution of MPTET is cooled from 20 to −30 °C, the emission wavelength remains unvaried at 435 nm, whereas the fluorescence intensity is increased because of the lowered thermal-induced nonradiative quenching efficiency (Figure 4, Figure S6 in the Supporting Information). When the solution is frozen at −50 °C, the maximum emission wavelength is red shifted to 560 nm. Further cooling of the sample does not change the red-shifted emission position. In dichloromethane solution of MPTET, the emission position keeps the same value as that at room temperature when the solution is cooled at −50 °C but red shifts to 560 nm when the solution is frozen to solid state at −100 °C. This suggests that the emission wavelength is dependent on not only the temperature but also the phase state of solution, that is, liquid or frozen state. Notably, the red-shifted emission positions of MPTET in the frozen acetonitrile and dichloromethane have the same value, which indicates that the excited state of MPTET relaxed to a similar structure in the frozen solution.

Similar fluorescence red shift sensitive to the solvent phase transition from liquid state to frozen state is also observed in MPTEP, MPTEO, and MPTEA but absent in MPTE (Table 4, Figure S7 in the Supporting Information). In particular, in the frozen solution, MPTEP, MPTET, MPTEO, and MPTEA exhibit similar emission behavior at around 560 nm, indicating that all fluorescent molecules with an aromatic ring adjacent to the triple bond share similar excited state structure in the frozen solution regardless of the electronic donating difference of the substituent.

Theoretical Calculations

Ground-State Structure in Solution. For better understanding of the spectra-related charge transfer processes, we also performed the theoretical calculations on the related MPT-derived fluorescent molecules. Notably, the structure of related molecules can be divided into three distinct fragments: the MPT

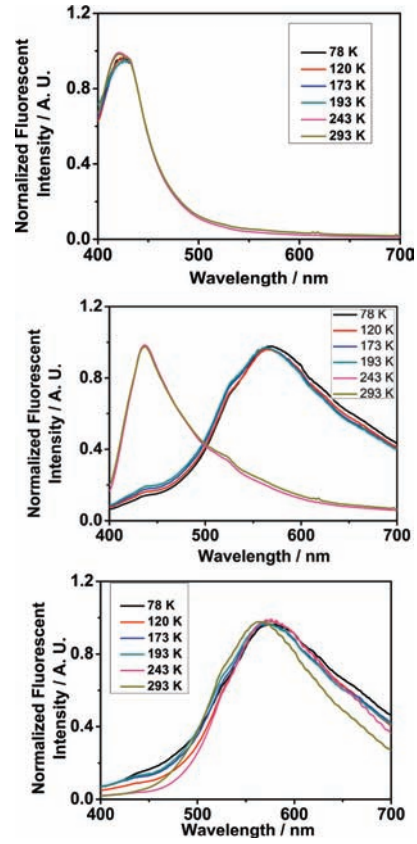

Figure 4. Normalized fluorescence spectra of MPTE (top), MPTET (middle), and MPTEA (bottom) in acetonitrile solution at different temperatures: 78, 120, 173, 193, 243, and 293 K. Each line is normalized according to its intensity maximum and smoothed through adjacent averaging method.

TABLE 4: Low-Temperature Fluorescence Spectra Data of the Related MPT Derivatives in Dichloromethane and Acetonitrile[17]

temperature	solvent	MPTE	MPTEP	MPTET	MPTEO	MPTEA
193 K	acetonitrile	426 nm	560 nm	565 nm	570 nm	567 nm
	dichloromethane	424 nm	434 nm	436 nm	435 nm	524 nm
120 K	acetonitrile	426 nm	560 nm	565 nm	570 nm	567 nm
	dichloromethane	425 nm	560 nm	565 nm	460 nm 570 nm	567 nm

moiety (fragment 1), the derived aromatic ring (fragment 2), and the donating substituent (fragment 3) with triple bond or single bond connecting the fragments. Ground-state structure optimization in vacuum produces a planar conformation for the current five fluorescent molecules (Figure 5). Different structural fragments, such as the derived aromatic ring, pyridine, and thiazole ring in 2-MPT moiety, keep good planarity in the ground state. The lone-pair electron of the donating substituent, such as the hydroxyl and amino group, is vertical to the aromatic ring. Selective structural parameters are listed in Table 5. Notably, the fragments retain similar structural parameters and are linked by a rotation-active single bond in distinct molecules, revealing that the differences in photophysical properties should result from the relative rotation between the structural fragments.

Two relative rotations are taken into account for further calculations. The rotation of fragment 2 around the single bond adjacent to fragment 1 is denoted as α rotation freedom, whereas the rotation freedom of fragment 3 around the single bond adjacent to fragment 2 is denoted as β rotation freedom. Different rotation freedoms exhibit distinct rotation barrier (Table 6). In vacuum, the α rotation freedom barrier (ΔE_α) for MPTEP, MPTET, MPTEO, and MPTEA is about 0.060, 0.034, 0.014, and 0.014 eV, whereas the β rotation barrier (ΔE_β) is about 0.046, 0.21, and 0.37 eV for MPTET, MPTEO, and MPTEA, respectively. Strong electron donor tends to have larger β rotation barriers, indicating that the electron donating strength is a key factor to dominate the β rotation barrier.

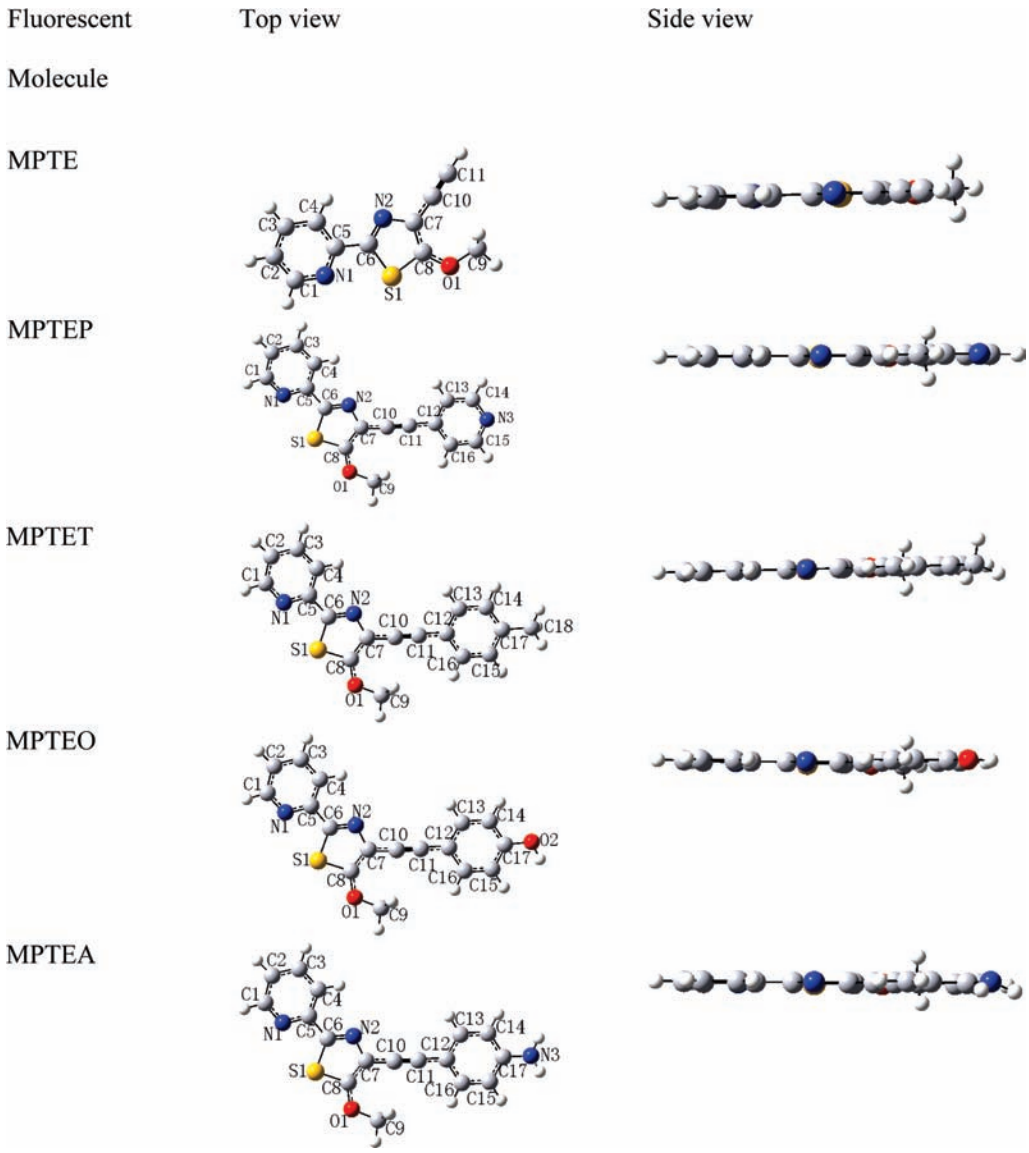

Figure 5. Optimized structure and atom labels for the related MPT derivatives in vacuum.

TABLE 5: Optimized Structural Parameters for the Related MPT Derivatives in Vacuum

parameter	MPTE	MPTEP	MPTET	MPTEO	MPTEA
C1−C2/Å	1.396	1.396	1.396	1.396	1.395
C2−C3/Å	1.396	1.396	1.396	1.396	1.397
C3−C4/Å	1.390	1.390	1.390	1.390	1.390
C4−C5/Å	1.403	1.403	1.403	1.403	1.404
C1−N1/Å	1.335	1.335	1.335	1.335	1.336
N1−C5/Å	1.344	1.344	1.344	1.344	1.344
C5−C6/Å	1.465	1.466	1.465	1.465	1.465
C6−N2/Å	1.298	1.297	1.298	1.298	1.298
N2−C7/Å	1.386	1.388	1.387	1.387	1.387
C7−C8/Å	1.392	1.395	1.394	1.393	1.392
C8−S1/Å	1.747	1.746	1.747	1.747	1.748
S1−C6/Å	1.766	1.768	1.767	1.766	1.766
C8−O1/Å	1.339	1.338	1.340	1.341	1.341
O1−C9/Å	1.434	1.434	1.433	1.432	1.434
C7−C10/Å		1.418	1.420	1.420	1.423
C10−C11/Å		1.217	1.217	1.217	1.217
C11−C12/Å		1.421	1.424	1.423	1.426
C12−C13/Å		1.409	1.410	1.411	1.409
C13−C14/Å		1.392	1.390	1.387	1.388
C12−C16/Å		1.408	1.408	1.408	1.409
C16−C15/Å		1.391	1.391	1.390	1.388
C4−C5−C6−N2/ degree	−0.013	0.000	−0.007	0.000	−0.073
N2−C7−C12−C13/ degree		0.000	0.000	0.005	0.000

The rotation barrier for α rotation freedom is approximate to the value of thermal perturbation ($\Delta E_\alpha \approx kT$, k is Boltzmann constant, whereas T is the temperature. kT value is ~0.026 eV at 300 K), suggesting that a twisted conformation with large α rotation angle can be populated at room temperature in both vacuo and polar solvents. In contrast, the high-energy β rotation freedom is difficult to be activated at room temperature, especially for those with strong electronic donors ($\Delta E_\beta \gg kT$, for MPTEO and MPTEA at 300 K), revealing a small β rotation angle at the ground-state structure, that is, nontwisted conformation, even at room temperature. This is in accordance with the absorption results, which suggest that the lone electron pair of nitrogen or oxygen atom contributes to the π orbitals. Herein, further calculations confine the conformation of β rotation freedom as frozen in nontwisted conformation.[18]

Calculated Electronic Transitions. In the ground state of the planar MPTE molecule, the frontier orbitals are delocalized π natured. The HOMO localizes on the triple bond and MPT moiety, whereas the LUMO localizes on the MPT moiety (Figure 6). TD-DFT calculations reveal that the $S_0 \rightarrow S_1$ transition from HOMO to LUMO is at 328 nm in acetonitrile. The computational results are in accordance with the absorption spectral results, which confirm that the electronic transitions arise between π-nature molecular orbitals.

The presence of the aromatic ring adds new distribution features to the molecular frontier orbitals. At the perpendicular conformation ground state ($\alpha = 90°$), the orthogonal π orbitals on each structural moiety, that is, fragments 1 and 2, slightly interact with each other, resulting in the distribution of π-nature HOMO-1 and HOMO mainly on either the MPT moiety, Ψ_1, or the aromatic ring, Ψ_{2+3}, depending on the energy levels (Figure 6). As a result, in the perpendicular conformation of MPTET, MPTEO, and MPTEA, HOMO-1 localizes on Ψ_{2+3} in vacuum, whereas in acetonitrile, HOMO-1 is altered on Ψ_1 in the perpendicular conformation of MPTEA. This may be due to the fact that the strong electronic donator amino group tends to gain more stabilization energy in polar solvents, which increases the energy level of the antibond (Ψ_{2+3}) between fragments 2 and 3. Upon the decrease in the α rotation angle, Ψ_{MPTE} interacts with $\Psi_{aromatic}$, which lowers the energy level of HOMO-1 but raises the energy level of HOMO (Figure 7a). The energy gap increase between HOMO-1 and HOMO when conformation is changed from orthogonal to planar is found to be 0.11, 0.71, 0.96, and 0.73 eV in MPTEP, MPTET, MPTEO, and MPTEA, respectively. The occupied frontier orbitals exhibit larger orbital delocalization in the nontwisted conformation than in the twisted conformation (Figure 6). Different from the HOMO and HOMO-1 with switchable orbital distribution, the LUMO in all five compounds mainly distributes on MPT skeleton in either the twisted or the nontwisted conformation and is slightly perturbed by α rotation freedom, which produces an insensitive energy level of LUMO to the α rotation angle. As a result, the energy gap between the HOMO and LUMO is decreased from 4.08 to 3.73 eV in MPTEA. A similar trend has also been found in other MPT-derived molecules. For MPTEP, MPTET, and MPTEO, their energy gap decrease from orthogonal to planar conformation is found to be 0.09, 0.28, and 0.39 eV, respectively.

TD-DFT calculations reveal the angular dependency of both the excitation wavelength and oscillator strength for the electronic transitions among frontier orbitals (Figure 7a−c). Upon the decrease in rotation angle, the first calculated excitation wavelength corresponding to the $S_0 \rightarrow S_1$ transition is red-shifted for MPTET, MPTEO, and MPTEA. The wavelength red-shifts when the conformation is changed from orthogonal to planar are calculated to be 22, 33, and 40 nm for MPTET, MPTEO, and MPTEA, respectively, and at each specific twisted angle, the excitation wavelength is increased in a sequence as MPTET < MPTEO < MPTEA. In contrast, the first calculated excitation wavelength for MPTEP is blue-shifted. MPTEP exhibits a smaller energy gap between fragment-1-based LUMO and fragment-2-based LUMO+1, which results in the simultaneous excitation from HOMO to LUMO and LUMO+1. The wavelength blue-shift when the conformation is changed from orthogonal to planar is calculated to be 13 nm. Compared with the experimental wavelength of the $S_0 \rightarrow S_1$ transition with the calculated angular dependency of excited wavelength, the twisted angle at room temperature is found to be about 68, 55, 67, and 75° for MPTEP, MPTET, MPTEO, and MPTEA, respectively. The twisted ground states of the related fluorescent molecules at room temperature further confirm the thermal-activated low-energy α rotation freedom. For both the planar and twisted geometry, the $S_0 \rightarrow S_1$ excitation process induces charge transfer from fragment 2 and 3 in HOMO to fragment 1 in LUMO, which suggests a PICT or TICT excited state at S_1, respectively. Solvent

TABLE 6: Rotation Barrier for α and β Rotation Freedom in the Related MPT Derivatives

	MPTEP	MPTET		MPTEO		MPTEA	
solvent	ΔE_α/eV	ΔE_α/eV	ΔE_β/eV	ΔE_α/eV	ΔE_β/eV	ΔE_α/eV	ΔE_β/eV
vacuum	0.060	0.034	0.046	0.014	0.21	0.014	0.37
dichloromethane	0.033	0.029	0.0048	0.019	0.22	0.010	0.44
acetonitrile	0.033	0.029	0.0047	0.020	0.22	0.010	0.46

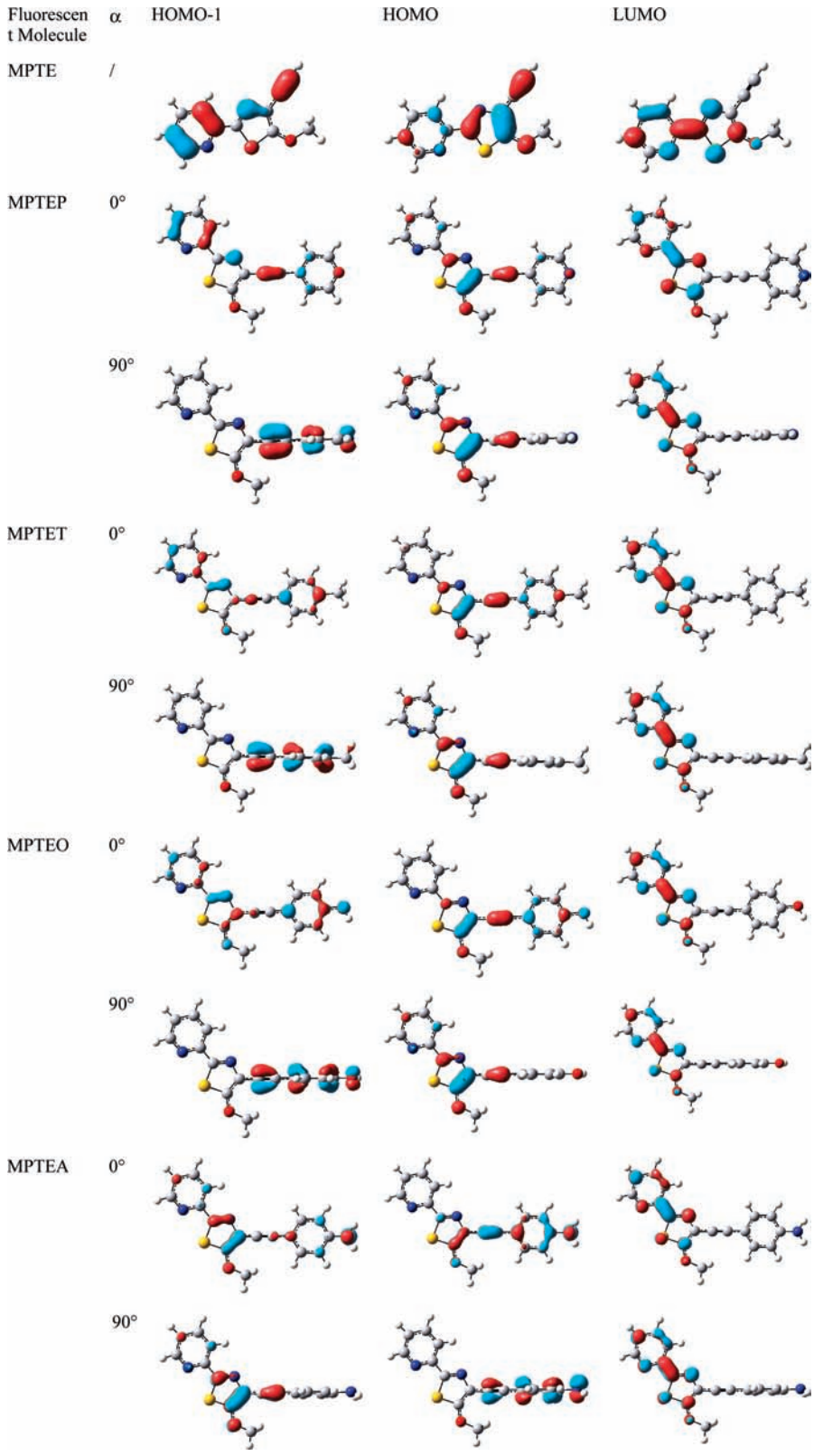

Figure 6. HOMO-1, HOMO, and LUMO molecular orbitals for the related MPT derivatives in acetonitrile with planar and twisted conformation.

polarity does not significantly affect the absorption wavelength for the related fluorescent molecules. When solvent is altered from acetonitrile to dichloromethane, the calculated wavelengths for the $S_0 \rightarrow S_1$ transition are slightly changed at each specific twisted angle for the MPT derivatives (Table 7), which are in accordance with the small absorption changes to the decrease in solvent polarity. More electronic transitions from S_0 to S_2 and higher energy orbitals have been calculated as the inner orbital transitions and match well with the experimental data (Table S7 in the Supporting Information). Notably, α rotation-dependent frontier-orbital nature is in accordance with the blue-shift fluorescence of MPTEA in PEG, which exhibits high viscosity to prevent the inner rotation of molecular fragments.

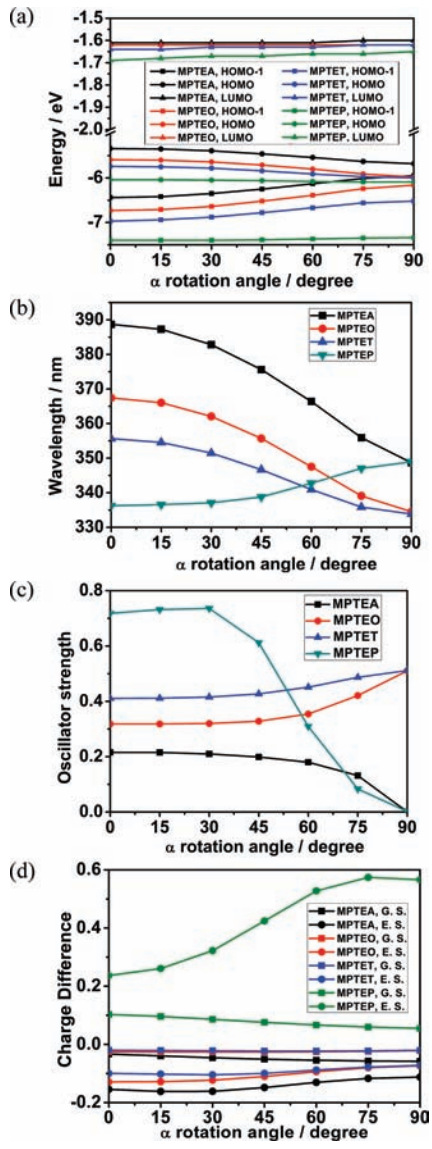

Figure 7. Plot of energy level for (a) HOMO-1, HOMO, and LUMO molecular orbitals, (b) calculated $S_0 \rightarrow S_1$ excitation wavelength, (c) calculated $S_0 \rightarrow S_1$ excitation oscillator strength, and (d) charge difference between fragment 1 and fragments 2 and 3 at both ground and excited states for the calculated $S_0 \rightarrow S_1$ excitation versus α rotation angle for MPTEP, MPTET, MPTEO, and MPTEA in acetonitrile. G. S.: ground state; E. S.: excited state.

Charge difference between fragment 1 and fragments 2 and 3 is also sensitive to α rotation freedom. At each specific rotation angle in acetonitrile, the charge difference at the excited state is more significant than that at the ground state for MPTEA, MPTEO, MPTET, and MPTEP (Figure 7d). This is in accordance with the fact that the charge-separated excited state originates from the $S_0 \rightarrow S_1$ excitation. Different from the negatively valued charge difference for MPTEA, MPTEO, and MPTET, the charge difference is positive for MPTEP. This is ascribed to the existence of strongly electronic withdrawing fragment 2. The $S_0 \rightarrow S_1$ excitation in MPTEP induces simultaneous excitation from the fragment-1-centered HOMO to the fragment-1-centered LUMO and fragment 2-centered LUMO+1, which further results in the negative charged fragment 2 and positive charged fragment 1 (Figure S8 in the Supporting Information) and, in turn, a positive charge difference. The charge difference value at the excited state is increased in a sequence of MPTEA < MPTEO < MPTET < MPTEP, which reveals that more electron density (negative charge) is donated to the fragment-1-centered LUMO orbitals upon excitation by strong electronic donators, such as amino, than by the weak donators, such as the methyl group.

Upon the decrease in rotation angle, α, the charge difference value at the Franck−Condon excited state becomes more negative, indicating that the charge transfer is enhanced alongside the $S_0 \rightarrow S_1$ excitation. This is ascribed to the fact that planar conformation is more favorable for charge transfer among the molecular skeleton. However, charge delocalization may also induce charge equalization among fragments to some extend, which might be responsible for the slight increase in the charge difference for MPTEA and MPTET when the α rotation angle is below 30°. As for MPTEP, a more planar structure is conducive to a decrease in the energy gap between HOMO and LUMO and favors the charge transfer to fragment-1-centered LUMO to decrease the positive value of the charge difference among fragments.

Emission Processes. On the basis of the spectral characterization and theoretical calculation, we may speculate the emission processes as follows. Because α rotation freedom produces an energy minimum at 0° in the energy surface of S_1 for MPTET, MPTEO, and MPTEA (for MPTEP, the energy minimum of S_1 is not at 0° because of the contribution of excitation from HOMO to LUMO+1, but from the view of the energy gap between the HOMO and LUMO, the energy minimum is still at 0°), the excited geometry would rotate around the triple bond axis to obtain a low-energy excited state. However, as for MPTET, MPTEO, and MPTEA in low polar solvents, α rotation freedom may not be activated in high viscosity solutions (e.g., PEG) and low polar solvents (e.g., *n*-hexane and ethyl acetate), which is evidenced by their characteristic emission at around 435 nm (Scheme 3). The relaxed S_1 state (TICT state) retains a twisted structure that is similar to that in the ground state. As for MPTEP, MPTET, MPTEO, and MPTEA, their rotation angles are similar, which suggests that increasing the electronic donating strength of the substituent may produce a larger dipole moment and lower energy relaxed excited state. The energy gap between frontier orbitals in the twisted excited conformation is larger than that in the planar excited conformation, which results in the fact that the emission band is mainly located at shorter than 500 nm in dichloromethane. The twisted excited state for TICT fluorescence generates from the twisted Franck−Condon excited state, and the relative fast excitation conformation change leads to the short fluorescence lifetimes of less than 0.4 ns for MPTEP, MPTET, MPTEO, and MPTEA in dichloromethane. The calculated excited-state dipole moments for TICT fluorescence of MPTEP, MPTET, MPTEO, and MPTEA are found to be less than 10 D. Especially for MPTEA, the excitation of $S_0 \rightarrow S_1$ promotes a charge transfer process from fragments 2 to 1 and exhibits a larger excited-state dipole moment than that in MPTEP, MPTET, and MPTEO, where the same excitation promotes the charge transfer mainly within fragment 1 and the triple bond. Consequently, the emission wavelength increases in a sequence as MPTEP < MPTET < MPTEO < MPTEA in dichloromethane.

For MPTEA in acetonitrile, the existence of a strong polar local site, for example, the amino group, tends to produce local solute−solvent interactions, stabilizing the more polar planar excited state.[7e] Local solute−solvent interactions have also been confirmed when a small amount of acetonitrile is added to viscous or low dipole solvent, resulting in the acetonitrile-specific fluorescence red shift. Strong local interaction for

TABLE 7: $S_0 \rightarrow S_1$ Excitation in Acetonitrile (A) and Dichloromethane (D) for the MPT Derivatives with Planar and Perpendicular Conformation

fluorescent molecule	solvent	α/degree	λ_{ex}/nm	E_{ex}/eV	oscillator strength	expansion coefficient	excited state
MPTE	A		329	3.77	0.4702	0.65824	HOMO → LUMO
	D		329	3.76	0.4831	0.65946	HOMO → LUMO
MPTEP	A	0	336	3.69	0.7182	0.49154	HOMO → LUMO+1
						−0.45929	HOMO → LUMO
	D	0	337	3.68	0.7378	0.48645	HOMO → LUMO+1
						−0.46630	HOMO → LUMO
	A	90	349	3.55	0.0013	0.68143	HOMO → LUMO+1
	D	90	349	3.55	0.0014	0.68124	HOMO → LUMO+1
MPTET	A	0	356	3.49	0.4105	0.66192	HOMO → LUMO
	D	0	357	3.48	0.4254	0.66240	HOMO → LUMO
	A	90	334	3.71	0.5115	0.65853	HOMO → LUMO
	D	90	335	3.70	0.5224	0.65977	HOMO → LUMO
MPTEO	A	0	367	3.37	0.3181	0.66950	HOMO → LUMO
	D	0	367	3.37	0.3358	0.66949	HOMO → LUMO
	A	90	334	3.71	0.5106	0.65861	HOMO → LUMO
	D	90	334	3.70	0.5219	0.65983	HOMO → LUMO
MPTEA	A	0	389	3.19	0.2156	0.67784	HOMO → LUMO
	D	0	388	3.20	0.2350	0.67723	HOMO → LUMO
	A	90	349	3.56	0.0003	0.70263	HOMO → LUMO
	D	90	345	3.59	0.0008	0.70233	HOMO → LUMO

SCHEME 2: Specific Rotation Freedom for Different Structural Moieties in the Related MPT Derivatives

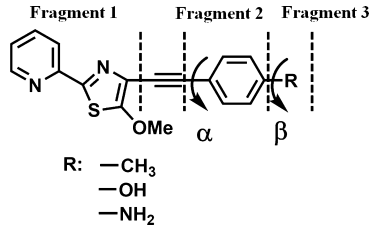

SCHEME 3: Scheme for the Excitation, Geometry Relaxation, and Emission of the TICT and PICT States in MPTEP, MPTET, MPTEO, and MPTEA

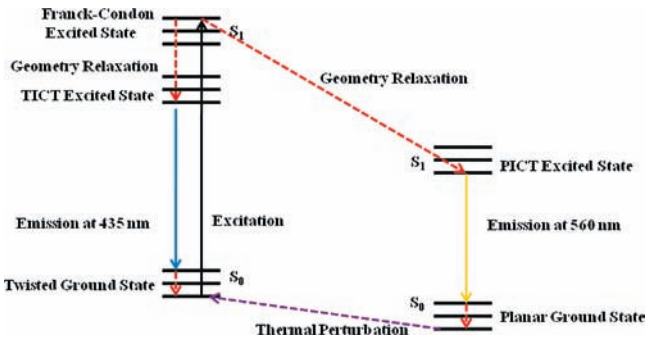

MPTEA overcomes the energy barrier in the solvent recombination process upon the relaxation of the Franck−Condon excited state and thus activates α rotation freedom to produce the PICT state. PICT conformation exhibits much lower occupied orbital energy than that in TICT. For a simple comparison, energy compensation by decreasing original double-occupied HOMO-1 for the increased energy of single-occupied HOMO is more effective in planar conformation because of the effective coupling of the HOMO-1 and HOMO, whereas the energy level of single-occupied LUMO remains unchanged (Figure 7a). Because of the smaller energy gap between frontier orbitals, the excited-state energy level in the planar conformation is lowered compared with that in the twisted conformation for MPTEA at room temperature in acetonitrile, which results in red-shifted emission maxima around 520 nm. The excited-state conformation change from the twisted Franck−Condon excited state to the planar excited state through the rotation of the aromatic ring for MPTEA at room temperature results in a fluorescence lifetime that is longer than 0.7 ns for PICT fluorescence of MPTEA. The nonradiative deactivation rate constant for PICT fluorescence at room temperature is also largely decreased compared with that for the TICT fluorescence, and the calculated excited-state dipole moment for PICT fluorescence of MPTEA is approximately 17 D. When the amino group is converted to its amide or protonated form, the lack of local solute−solvent interactions denies the relative rotation of the aromatic ring and blocks the activation of the PICT state.

In a frozen solution, low temperature and, in particular, solvent lattice constraints limit MPTEP, MPTET, MPTEO, and MPTEA with planar and excited ground states, which activates the PICT state with characteristic emission at 560 nm in response to the solution phase transition from liquid to solid state upon being frozen. Notably, MPTE retains the same excited and ground states upon the solution phase transition from liquid to solid state upon being frozen and lacks solution-phase-sensitive fluorescence.

Conclusions

In conclusion, charge transfer processes in a series of MPT-derived fluorescent molecules with either donor or acceptor substituent are investigated in the present article. This is the first time a fluorescence-substituent correlation is investigated in the blue-emissive 2-MPT fluorophore, and different roles of substituents are discussed. When an aromatic ring is adjacent to the end of triple bond, the rotation of the aromatic ring around the triple-bond axis endows the fluorescent molecules with different ground- and excited-state conformation. At room temperature, the ground-state structure is in an aromatic ring-twisted conformation because of thermal perturbation. At excited state, the emission from a twisted conformation produces the fluorescence maxima at around 435 nm; whereas, the emission from a planar conformation results in the red shift of fluorescence maxima at around 560 nm. In PICT state, aromatic ring and MPT moiety are efficiently coupled to produce a small energy gap between frontier orbitals. The introduction of the strong electronic donator, that is, the amino group, tends to assist

the transition from the twisted excited state to the planar one in polar solvents through local interactions. Other substituents from the weak donor (e.g., methyl group in MPTET) and strong donor (e.g., hydroxyl group in MPTEO) cannot achieve the same transition at room temperature. When temperature is below the frozen point, the fluorescent molecule is constrained to a planar conformation by solvent lattice, resulting in the activation of PICT emission at 560 nm for the aromatic-conjugated MPT derivatives with a solution-phase-sensitive fluorescence switching.

Acknowledgment. We acknowledge the support for this research through the NSFC under contract numbers 20821091 and 20771009 and through Peking University.

Supporting Information Available: Additional spectral, Cartesian geometries for the optimized structure, and computational details. This material is available free of charge via the Internet at http://pubs.acs.org.

References and Notes

(1) (a) de Silva, A. P.; Gunnlaugsson, H. Q. N.; McCoy, C. P. *Nature* **1993**, *364*, 42–44. (b) de Silva, A. P.; McClenaghan, N. D.; McCoy, C. P. Molecular-Level Electronics, Imaging and Information, Energy and Environment. In *Electron Transfer in Chemistry*; Balzani, V., Ed.; Wiley-VCH: Weinheim, Germany, 2001; Vol. 5. (c) Balzani, V.; Venturi, M.; Credi, A. *Molecular Devices and Machines A Journey into the Nano World*; Wiley-VCH: Weinheim, Germany, 2003. (d) de Silva, A. P. *Nat. Mater.* **2005**, *4*, 15–16. (e) de Silva, A. P.; Uchiyama, S. *Nat. Nanotechnol.* **2007**, *2*, 399–410. (f) Ballardin, R.; Ceroni, P.; Credi, A.; Gandolfi, M. T.; Maestri, M.; Semararo, M.; Venturi, M.; Balzani, V. *Adv. Funct. Mater.* **2007**, *17*, 740–750. (g) Balzani, V.; Credi, A.; Venturi, M. *Chem.—Eur. J.* **2008**, *14*, 26–39.

(2) (a) Brown, G. J.; de Silva, A. P.; Pagliari, S. *Chem. Commun.* **2002**, 2461–2463. (b) de Silva, A. P.; McClenaghan, N. D. *Chem.—Eur. J.* **2002**, *8*, 4935–4945. (c) Raymo, F. M.; Giordani, S. *Proc. Natl. Acad. Sci. U.S.A.* **2002**, *99*, 4941–2944. (d) de Silva, A. P.; McCaughan, B.; McKinney, B. O. F.; Querol, M. *Dalton Trans.* **2003**, 1902–1913. (e) de Silva, A. P.; McClenaghan, N. D. *Chem.—Eur. J.* **2004**, *10*, 574–586. (f) Guo, X. F.; Zhang, D. Q.; Zhu, D. B. *Adv. Mater.* **2004**, *16*, 125–130. (g) Qu, D. H.; Ji, F. Y.; Wang, Q. C.; Tian, H. *Adv. Mater.* **2006**, *18*, 2035–2038. (h) Zhou, W. D.; Li, Y. J.; Li, Y. L.; Liu, H. B.; Wang, S.; Li, C. H.; Yuan, M. J.; Liu, X. F.; Zhu, D. B. *Chem. Asian J.* **2006**, *1*−*2*, 224–230.

(3) (a) Gust, D.; Moore, T. A.; Moore, A. L. *Chem. Commun.* **2006**, 1169–1178. (b) Biancardo, M.; Bignozzi, C.; Doyle, H.; Redmond, G. *Chem. Commun.* **2005**, 3918–3920. (c) Raymo, F. M.; Tomasulo, M. *J. Phys. Chem. A* **2005**, *109*, 7343–7352. (d) Li, F. Y.; Shi, M.; Huang, C. H.; Jin, L. P. *J. Mater. Chem.* **2005**, *15*, 3015–3020. (e) Zhou, Y.; Wu, H.; Qu, L.; Zhang, D. Q.; Zhu, D. B. *J. Phys. Chem. B* **2006**, *110*, 15676–15679.

(4) (a) Balzani, V.; Credi, A.; Venturi, M. *ChemPhysChem* **2003**, *3*, 49–59. (b) de Silva, A. P.; Gunaratne, H. Q. N.; Gunnlaugsson, T.; Huxley, A. J. M.; McCoy, C. P.; Rademacher, J. T.; Rice, T. E. *Chem. Rev.* **1997**, *97*, 1515–1566.

(5) Irie, M.; Fukaminato, T.; Saski, T.; Tamai, N.; Kawai, T. *Nature* **2002**, *420*, 759–760.

(6) (a) Kollmannsberger, M.; Rurack, K.; Resch-Genger, U.; Daub, J. *J. Phys. Chem. A* **1998**, *102*, 10211–10220. (b) Coskun, A.; Deniz, E.; Akkaya, E. U. *Org. Lett.* **2005**, *7*, 5187–5189. (c) Xue, H.; Tang, X. J.; Wu, L. Z.; Zhang, L. P.; Tung, C. H. *J. Org. Chem.* **2005**, *70*, 9727–9734. (d) García-Acosta, B.; Martínez-Máñez, R.; Sancenón, F.; Soto, J.; Rurack, K.; Spieles, M.; García-Breijo, E.; Gil, L. *Inorg. Chem.* **2007**, *46*, 3123–3135.

(7) (a) ValeurB. *Molecular Fluorescence: Principles and Applications*; Wiley-VCH: Weinheim, Germany, 2002. (b) Suzuki, K.; Tanabe, H.; Tobita, S.; Shizuka, H. *J. Phys. Chem. A* **1997**, *101*, 4496–4503. (c) Grabowski, Z. R.; Rotkiewicz, K.; Rettig, W. *Chem. Rev.* **2003**, *103*, 3899–4031. (d) Nad, S.; Kumbhakar, M.; Pal, H. *J. Phys. Chem. A* **2003**, *107*, 4808–4816. (e) El-Gezawy, H.; Rettig, W.; Lapouyade, R. *J. Phys. Chem. A* **2006**, *110*, 67–75. (f) Resch-Genger, U.; Li, Y. Q.; Bricks, J. L.; Kharlanov, V.; Rettig, W. *J. Phys. Chem. A* **2006**, *110*, 10956–10971.

(8) Zheng, M. H.; Jin, J. Y.; Sun, W.; Yan, C. H. *New J. Chem.* **2006**, *30*, 1192–1196.

(9) (a) Fang, C. J.; Zhu, Z.; Sun, W.; Xu, C. H.; Yan, C. H. *New J. Chem.* **2007**, *31*, 580–586. (b) Sun, W.; Zheng, Y. R.; Xu, C. H.; Fang, C. J.; Yan, C. H. *J. Phys. Chem. C* **2007**, *111*, 11706–11711. (c) Li, Z. X.; Liao, L. Y.; Sun, W.; Xu, C. H.; Zhang, C.; Fang, C. J.; Yan, C. H. *J. Phys. Chem. C* **2008**, *112*, 5190–5196. (d) Sun, W.; Zhou, C.; Xu, C. H.; Fang, C. J.; Zhang, C.; Li, Z. X.; Yan, C. H. *Chem.—Eur. J.* **2008**, *14*, 6342–6351. (e) Sun, W.; Xu, C. H.; Zhu, Z.; Fang, C. J.; Yan, C. H. *J. Phys. Chem. C* **2008**, *112*, 16973–16983.

(10) Demas, J. N.; Grosby, G. A. *J. Phys. Chem.* **1971**, *75*, 991–1024.

(11) (a) Frisch, M. J.; Trucks, G. W.; Schlegel, H. B.; Scuseria, G. E.; Robb, M. A.; Cheeseman, J. R.; Montgomery, J. A., Jr.; Vreven, T.; Kudin, K. N.; Burant, J. C.; Millam, J. M.; Iyengar, S. S.; Tomasi, J.; Barone, V.; Mennucci, B.; Cossi, M.; Scalmani, G.; Rega, N.; Petersson, G. A.; Nakatsuji, H.; Hada, M.; Ehara, M.; Toyota, K.; Fukuda, R.; Hasegawa, J.; Ishida, M.; Nakajima, T.; Honda, Y.; Kitao, O.; Nakai, H.; Klene, M.; Li, X.; Knox, J. E.; Hratchian, H. P.; Cross, J. B.; Bakken, V.; Adamo, C.; Jaramillo, J.; Gomperts, R.; Stratmann, R. E.; Yazyev, O.; Austin, A. J.; Cammi, R.; Pomelli, C.; Ochterski, J.; Ayala, P. Y.; Morokuma, K.; Voth, G. A.; Salvador, P.; Dannenberg, J. J.; Zakrzewski, V. G.; Dapprich, S.; Daniels, A. D.; Strain, M. C.; Farkas, O.; Malick, D. K.; Rabuck, A. D.; Raghavachari, K. J.; Foresman, B.; Ortiz, J. V.; Cui, Q.; Baboul, A. G.; Clifford, S.; Cioslowski, J.; Stefanov, B. B.; Liu, G.; Liashenko, A.; Piskorz, P.; Komaromi, I.; Martin, R. L.; Fox, D. J.; Keith, T.; Al-Laham, M. A.; Peng, C. Y.; Nanayakkara, A.; Challacombe, M.; Gill, P. M. W.; Johnson, B. G.; Chen, W.; Wong, M. W.; Gonzalez, C.; Pople, J. A. *GAUSSIAN 03*, revision B.05; Gaussian, Inc.: Pittsburgh, PA, 2003. (b) Hay, P. J.; Wadt, W. R. *J. Chem. Phys.* **1985**, *82*, 270–283. (c) Hay, P. J.; Wadt, W. R. *J. Chem. Phys.* **1985**, *82*, 299–310. (d) Wadt, W. R.; Hay, P. J. *J. Chem. Phys.* **1985**, *82*, 284–298. (e) Lee, C.; Yang, W.; Parr, R. G. *Phys. Rev. B* **1988**, *37*, 785–789. (f) Adamo, C.; Barone, V. *Chem. Phys. Lett.* **2000**, *330*, 152–160. (g) Jodicke, C. J.; Luthi, H. P. *J. Chem. Phys.* **2002**, *117*, 4146–4156. (h) Scholz, R.; Kobitski, A. Y.; Zahn, D. R. T.; Schreiber, M. *Phys. Rev. B* **2005**, *72*, 245208–245225. (i) Neiss, C.; Saalfrank, P.; Parac, M.; Grimme, S. *J. Phys. Chem. A* **2003**, *107*, 140–147.

(12) Jia, C. Y.; Liu, S. X.; Tanner, C.; Leiggener, C.; Neels, A.; Sanguinet, L.; Levillain, E.; Leutwyler, S.; Hauser, A.; Decurtins, S. *Chem.—Eur. J.* **2007**, *13*, 3804–3812.

(13) Maus, M.; Rettig, W.; Bonafoux, D.; Lapouyade, R. *J. Phys. Chem. A* **1999**, *103*, 3388–3401.

(14) Chakraborty, A.; Kar, S.; Nath, D. N.; Guchhait, N. *J. Phys. Chem. A* **2006**, *110*, 12089–12095.

(15) (a) Mataga, N.; Kaifu, Y.; Koizumi, M. *Bull. Chem. Soc. Jpn.* **1956**, *29*, 465–470. (b) El-Gezawy, H.; Rettig, W.; Lapouyade, R. *J. Phys. Chem. A* **2006**, *110*, 67–75.

(16) Yang, J. S.; Liao, K. L.; Hwang, C. Y.; Wang, C. M. *J. Phys. Chem. A* **2006**, *110*, 8003–8010.

(17) The emission wavelengths measured at low temperature are different from those measured at room temperature, even in the fluid solution. This may due to the differences in instrument apparatus. For measuring low-temperature fluorescence spectra, a Jobin-Yvon HR800 Raman spectrometer (France) with a 325 nm laser excitation source was used, whereas for measuring room-temperature fluorescence spectra, a Hitachi F4500 spectrometer is used. However, the trends of the changes in emission wavelength are still clear. For MPTEP, MPTET, MPTEO, and MPTEA, their emission wavelength maxima are red shifted upon the solution phase transition from liquid state to solid state upon being frozen. For MPTE, the same red shift cannot be observed. When the solution is frozen, the cooling speed is important for the emission maxima. If the cooling speed is fast, then some molecules will be frozen in their original conformation in fluid solvent, which still emits at shorter wavelength. This is the reason that MPTEO emits two peaks in the frozen dichloromethane solution at 120 K. However, in most cases, we do not observe the dual emission behavior seen in MPTEO.

(18) Stsiapura, V. I.; Maskevich, A. A.; Kuzmitsky, V. A.; Turoverov, K. K.; Kuznetsova, I. M. *J. Phys. Chem. A* **2007**, *111*, 4929–4835.

JP9007224